agronomy

MDPI

The Utility of the Upcoming HyspIRI's Simulated Spectral Settings in Detecting Maize Gray Leafy Spot in Relation to Sentinel-2 MSI, VENµS, and Landsat 8 OLI Sensors

Mbulisi Sibanda [1],* , Onisimo Mutanga [1] , Timothy Dube [2], John Odindi [1] and Paramu L. Mafongoya [3]

[1]   Discipline of Geography, School of Agricultural Earth and Environmental Sciences, University of KwaZulu-Natal, Private Bag X01, Pietermaritzburg 3209, South Africa; MutangaO@ukzn.ac.za (O.M.); Odindi@ukzn.ac.za (J.O.)

[2]   Institute for Water Studies, Department of Earth Sciences, The University of the Western Cape, Private Bag X17, Bellville 7535, South Africa; tidube@uwc.ac.za

[3]   Discipline of Agronomy and Rural Development, School of Agricultural Earth and Environmental Sciences, University of KwaZulu-Natal, Private Bag X01, Pietermaritzburg 3209, South Africa; Mafongoya@ukzn.ac.za

*   Correspondence: sibandam3@ukzn.ac.za; Tel.: +27-33-260-5345

check for updates

Abstract: Considering the high maize yield loses caused by incidences of disease, as well as incomprehensive monitoring initiatives in crop farming, there is a need for spatially explicit, cost-effective, and consistent approaches for monitoring, as well as for forecasting, food-crop diseases, such as maize Gray Leaf Spot. Such approaches are valuable in reducing the associated economic losses while fostering food security. In this study, we sought to investigate the utility of the forthcoming HyspIRI sensor in detecting disease progression of Maize Gray Leaf Spot infestation in relation to the Sentinel-2 MSI and Landsat 8 OLI spectral configurations simulated using proximally sensed data. Healthy, intermediate, and severe categories of maize crop infections by the Gray Leaf Spot disease were discriminated based on partial least squares–discriminant analysis (PLS-DA) algorithm. Comparatively, the results show that the HyspIRI's simulated spectral settings slightly performed better than those of Sentinel-2 MSI, VENµS, and Landsat 8 OLI sensor. HyspIRI exhibited an overall accuracy of 0.98 compared to 0.95, 0.93, and 0.89, which were exhibited by Sentinel-2 MSI, VENµS, and Landsat 8 OLI sensor sensors, respectively. Furthermore, the results showed that the visible section, red-edge, and NIR covered by all the four sensors were the most influential spectral regions for discriminating different Maize Gray Leaf Spot infections. These findings underscore the potential value of the upcoming hyperspectral HyspIRI sensor in precision agriculture and forecasting of crop-disease epidemics, which are necessary to ensure food security.

Keywords: hyperspectral data; maize; crop diseases; PLS-DA

1. Introduction

In Sub-Saharan Africa, maize is the most important cereal crop farmed on over 25 million ha, mainly by smallholder farmers. These smallholder maize farms yield beyond 38 million metric tons of grain, mainly for subsistence purposes [1]. The production of maize has however largely been stalled by pests and diseases that affect maize crops during the growing, post-harvesting processing, and storage stages.

Gray Leaf Spot (GLS) is one of the major diseases that adversely affects maize crop production. The disease is caused by a *Cercospora zeae-maydis* fungus, which affects maize crops across all the

phenological stages. According to Dhami, et al. [2], *Cercospora zeae-maydis* is a polycyclic facultative pathogen or fungi which survives as mycelium in the residues of infected maize crops after harvesting. The conidia infect the maize crops through the stomatal openings of leaves. Approximately two to three weeks after colonizing maize leaf tissues, gray-to-tan lesions grow between the leaf veins, giving them a narrow rectangular appearance, which is 5–70 mm long by 2–4 mm wide [2]. These lesions ultimately sporulate, spread, and coalesce, covering the entire leaf surface area. Subsequently, these lesions excessively reduce the level of sugar, causing stalk lodging, which ultimately results in premature death or extreme yield losses of up to 100% [2]. In this regard, despite the fact that it can be managed through the utilization of resistant hybrids, crop rotations, tillage practices, and, if need be, the use of foliar-applied fungicides, the GLS is widely recognized as the most significant yield-limiting disease in maize crop production, [3–5]. Therefore, efficient novel techniques for forecasting pandemics similar to GLS are necessary to foster food security, especially in the developing countries in Sub-Saharan Africa, where maize farming is the mainstay of millions of livelihoods.

In developing countries, it is currently a common practice for farmers to rely on field surveys to monitor the health of agricultural crops such as maize [6]. Furthermore, the administration of agrochemicals to treat fungal pathogen disease, such as GLS, is also currently conducted in an indiscriminate manner, which results in exorbitant economic losses associated with purchasing and applying fungicides. Such techniques of administering agrochemicals also result in excessive pollution of proximal stream and underground water sources [7]. Furthermore, the estimation of damages associated with such epidemic crop diseases, including their spatial extent, as well as their real-time spatial distribution, have largely been contingent on physical surveys. However, techniques such as physical surveys have proved to be highly subjective, tedious, relatively time-consuming, and unreliable at landscape scales, especially when preparing for the next cropping season [6]. Subsequently, there is a need for cheap, fast, and consistent methods for agricultural-crop-disease monitoring, as well as forecasting of related food-crop diseases, for fostering food security while reducing the associated economic losses, as well as environmental pollution from the indiscriminate administration of pesticides. Above all, such efficient techniques for agricultural-crop-disease monitoring will provide the critically necessary information for decision making, particularly in determining the need for timely administration of agrochemicals, to reduce yield losses.

To date, earth observation techniques have been widely proven to be an effective noninvasive, nondestructive, and autonomous tool for detecting and monitoring biotic and abiotic stress in agricultural crops at local to regional scales and different phenological stages [7–10]. The success of remotely sensed data in monitoring and forecasting crop diseases such as GLS stems from its synoptic views, which offer timely acquired, spatially explicit, continuous, and abundant wavebands, with the ability to detect subtle biochemical and physical changes of crop plants. Earth observation sensors record the spectral reflectance of plant canopies of both infected and healthy crops. Subsequently, the spectral signature of infected crops tends to be different from that of healthy crops due to the biochemical and physiological alterations caused by crop diseases such as GLS [11–16]. The infection of crop plants results in the alteration of spectral reflectance, mainly due to the perpetual diminution of chlorophyll content, as well as the modification of internal tissue structure, which, in turn, results in physiological changes in the canopy of the crops [11]. When a plant is infected, the disease-stress reduces the chlorophyll concentration, which results in increased reflectance in the red region of the electromagnetic spectrum (EMS) [11]. Comparatively, healthy crop plants are associated with a high reflectance in the green and near-infrared spectrums and low reflectance in the red and blue spectrums [11]. Furthermore, the increase in the magnitude of infection specifically alters numerous leaf optical properties, such as the leaf angle distribution (LAD), leaf area index (LAI), and the biomass of a plant, which directly influence and determine the target-energy interactions (i.e., energy absorption, reflectance, and transmission) in remote-sensing vegetation. Subsequently, maize crop farming could benefit from the timeous, spatially explicit wall-to-wall detection and monitoring system offered by remote-sensing techniques, which reduces costs and ensures food security [13,17].

Hyperspectral sensors have been proven to be the most robust and accurate sources of remotely sensed data in vegetation-mapping studies, particularly agricultural crops [17–22]. For instance, Calderón, Navas-Cortés, and Zarco-Tejada [22] illustrated that hyperspectral remotely sensed data could accurately discriminate Verticillium Wilt diseases on olive crops, with optimal overall accuracies of 71.4% and 75.0% at the initial and severe stages of infection. The high discrimination accuracies in crops at different levels of infection associated with hyperspectral data are attributed to its narrow spectral channels, which have the ability to capture minute spectral variations induced by crop diseases at various stages, which are otherwise masked by broad multispectral sensors. However, hyperspectral data are often costly and have high data dimensionality, while being limited to local-scale applications. Hence, the rapid development of sensor technologies and the emergence of freely available broadband sensors have raised a lot of interest in favor of sensor missions, such as Landsat. Specifically, the recently launched Landsat Operational Land imager (OLI) has been of significant interest in agricultural crops mapping studies. Although Landsat data perform satisfactorily in mapping agricultural crop traits at landscape scales, their broad wavebands does not adequately cover portions of the EMS that are critical in vegetation mapping, such as the red edge. This limitation resulted in the emergence of Sentinel-2 multispectral imager (MSI), as well as the Vegetation and Environment monitoring on a New MicroSatellite (VENμS), as better alternatives in the remote sensing of crop diseases, such as GSL. Furthermore, the earth observation community is eagerly awaiting hyperspectral sensors which will offer free data at relatively large spatial scales, such as the Indian Space Research Organization's Geostationary Hyperspectral Imager Satellite (GISAT), Italy/Israel's Shalom, Germany's Environmental Mapping and Analysis Program (EnMap), and the National Aeronautics and Space Administration's (NASA) Hyperspectral InfraRed Imager (HyspIRI) [21].

The HyspIRI sensor will be characterized by two instruments with an intelligent payload module: Visible/near infrared/Shortwave InfraRed (VSWIR) imaging spectrometer and a thermal infrared (TIR) multispectral imager. The sensor will offer global coverage data at 5 and 16 days and temporal resolutions of 30 and 60 m spatial resolution [23–26]. Such a temporal resolution is optimal for monitoring diseases with relatively longer latent periods, such as GLS, which can take as long as 14 to 28 days after infection for the lesions to sporulate [2,27,28]. Above all, the VSWIR instrument will offer 7 nm narrow contiguous wavebands perceived to be sensitive to the detection and mapping of crop diseases to increase yields and surpass food insecurities. Hyperspectral sensors such as HyspIRI offer specific narrow spectral channels, which are suitable for targeted monitoring of specific optical biochemical and physical plant parameters, before and after infection by diseases, at relatively low costs [25,29]. Nonetheless, there is still a highly significant knowledge gap in the full exploitation of hyperspectral remotely sensed data, especially in the crop farming. Since the inception of NASA's HyspIRI mission, there has been a call for comparative studies to assess the performance of HyspIRI's spectral settings and other hyper and multispectral sensors so as to advance our knowledge and models in vegetation-health characterization [21]. It is against this background that this study seeks to assess the strength and the practicality of simulated HyspIRI's spectral configuration in detecting and discriminating maize crops at various levels of Maize Gray Leaf Spot (MGLS) diseases infection levels in relation to Sentinel-2MSI, VENμS, and Landsat OLI.

2. Methods and Materials

2.1. Crop Description and Experimental Site

The Cedara College of Agriculture maize farm in KwaZulu Natal South Africa (29°32′0″ South, 30°16′0″ East) (Figure 1) was use used as a site for the study. Cedara is situated in the Moist Midlands Mist belt of KwaZulu Natal province in South Africa. The area is characterized by an altitude that ranges between 900 and 1400 m above sea level. It is a hilly and rolling country with a high percentage of arable land (i.e., 47% is of the area is suitable for cropping). Soils are relatively deep, highly leached, and strongly acidic. Fertility is low, but physical properties are favorable. Mean maximum January

temperature for the research station is 25 °C, while mean minimum July temperature is 4 °C. The area is generally rich in water resources, with rainfall of about 900 mm/annum.
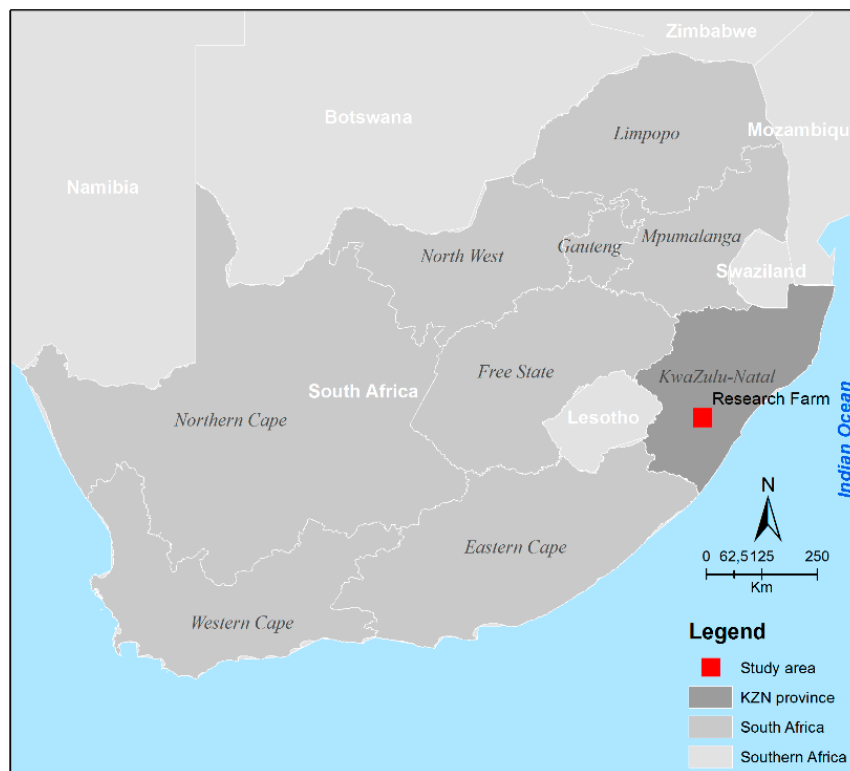
Figure 1. The general location of the Research Farm in Pietermaritzburg, KwaZulu Natal Province, South Africa.

The crop was planted on 25 February 2014, on 122 plots, under the evaluation/supervision of an agronomist. A total of 62 plots had the GLS inoculated on maize crops, while 60 plots had healthy, untreated maize crops. The plots were 3 m by 3 m, with intra-row spacing and row lengths of 0.75 m and 0.3 m, respectively. The number of plants ranged between 15 and 20 plants per plot. Infected maize crops were visually assessed and determined with aide of agronomists and spectral measurements that were conducted twice during the peak phenological stage of maize growth. Figure 2a–c illustrates the samples characterized as the healthy, moderately infected, and severely infected stages, respectively. In this study, the leaves that exhibited no traces of GLS lesions were referred to as "healthy" while leaves that had 10%–42% lesions were referred to as "intermediately" infected. Leaves which exhibited 43% to 100% coverage by GLS lesions were referred to as severely infected. Spectral reflectance measurements were recorded and labeled in the same manner. The density of lesions in infected plants was used to define the thresholds 10%–42% and 43%–100% between intermediately and severely infected crop plants. The total leaf area for all the maize crops were above one square meter, their mean length was 80 cm, and their mean width was 9.8 cm.
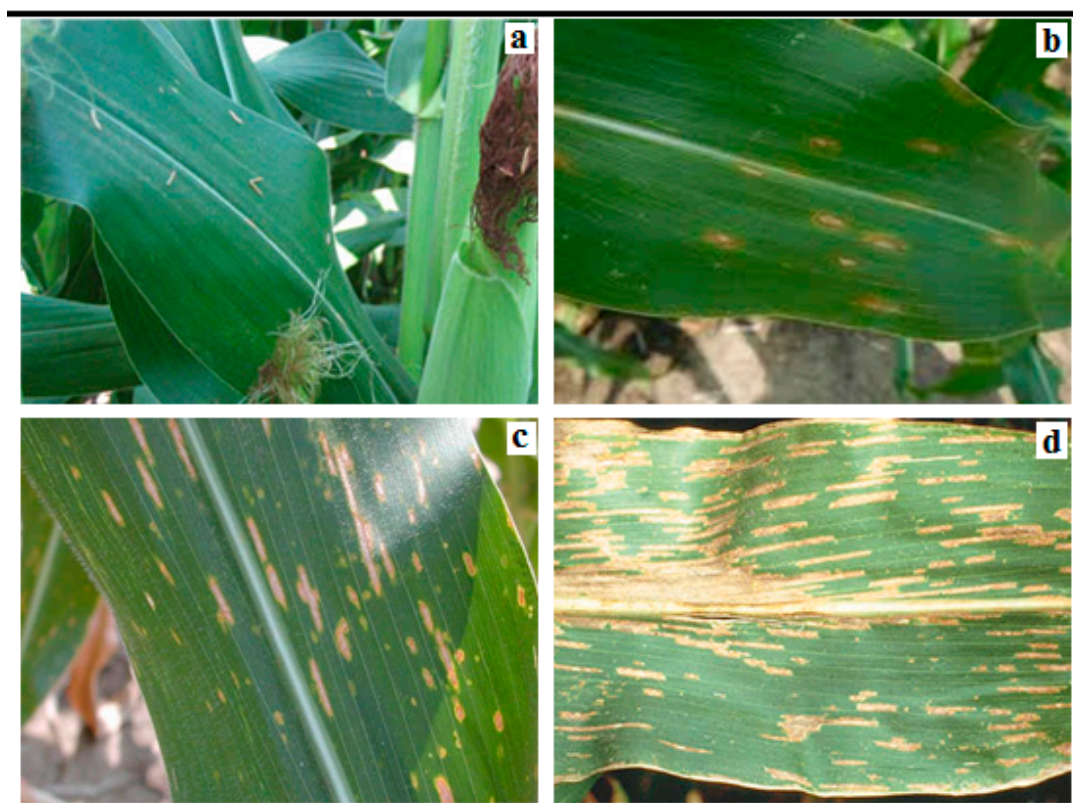
Figure 2. Maize leaves that are (**a**) healthy, and (**b**,**c**) intermediately and (**d**) severely infected by Grey Leaf Spot disease.

2.2. Remotely Sensed Data

An analytical spectral device (ASD) FieldSpec® 4 optical sensor (former Analytical Spectral Devices, Inc., Boulder, CO, USA now Malvern Panalytical Ltd.) was used to measure the spectral reflectance of maize crops under different levels of GLS disease infections. Reflectance measurements were recorded at 1.4 nm intervals between the 350 and 1000 nm regions, as well as 2 nm intervals between the 1000 to 2500 nm regions. Bare fiber optic linked to the ASD instrument was held at near-nadir position at the canopies of maize plants under different levels of infection. The sensor was held at an average height of about 0.2 m away from the canopies of crops, resulting in a field of view with a diameter of approximately 0.15 m. The spectral measurements were conducted by one person, in order to avoid inconsistencies. Spectral measurements were normalized after every 5 to 10 spectral measurements, using a standard white spectralon to circumvent the possible changes in weather conditions, as well as irradiance from the sun. Fifty-three spectral samples were measured under each level of infection (total samples $n = 159$). Spectral measurements were conducted between 10:00 and 14:00 h, under clear sky conditions, as that is the time of the day with maximum net radiation from the sun. The spectra were then resampled to the spectra settings of HyspIRI, Sentinel-2 MSI, VENµS, and Landsat OLI sensors.

Resampling ASD Data to the Spectral Band Settings of HyspIRI, Sentinel-2MSI, VENµS, and Landsat OLI

To simulate HyspIRI spectra band settings, a weighted average based on adjacent bands of the original proxy hyperspectral data were used to simulate each HyspIRI VSWIR waveband. According to Prasad, et al. [30], in the absence of the actual HyspIRI VSWIR modulation transfer function, weights for such an averaging procedure can be assumed to follow a Gaussian shape. The width of the Gaussian shape is determined by the full-width-half-maximum (FWHM) bandwidth of the HyspIRI VSWIR

sensor. Consequently, the field measured proxy hyperspectral sensor data were simulated from a spectral range from 380 to 2500 nm, at a sampling interval of 10 nm, based on the planned specifications of the HyspIRI sensor [31]. In simulating broadband spectral sensors (i.e., Sentinel-2 MSI, VENμS, and Landsat OLI sensors), PRISM in IDL-ENVI was utilized. PRISM in IDL-ENVI also takes into consideration the full-width-half-maximum (FWHM) bandwidth of each of these broadband sensors.

2.3. Statistical Analysis

A two-phased approach was adopted in this study to determine the strength of HyspIRI in relation to Sentinel-2 MSI, VENμS, and Landsat OLI spectral settings in statistically discriminating maize crops that are healthy, and intermediately and severely infected by Grey Leaf Spot disease. In the first phase, analysis of variance was conducted in discriminating the reflectance of maize crops under different GLS infection levels across the four spectral settings. In the second phase, partial least squares–discriminant analysis (PLS–DA) was used to discriminate the reflectance of maize crops under different GLS infection levels based on the spectral settings of the four sensors. PLS–DA was selected and used in this study because it has the ability to circumvent high dimensionality associated with hyperspectral datasets, such as that of HyspIRI, while reducing the risk of overfitting models. Above all, PLS–DA has the ability to discern the most influential variables in the latent factors with optimal discriminations. The classifications were conducted in Microsoft XlStat statistical package.

2.4. Accuracy Assessment

Prior to discrimination based on PLS–DA, the data were split into 70% training and 30% testing datasets. The cross-validated confusion matrices were derived and used to compute the overall, user, and producer accuracies for the four sensors' spectral settings. In that regard, the overall, user, and producer accuracies were used in assessing the strength of HyspIRI's spectral configuration in detecting and discriminating various GLS infection levels in relation to that of Sentinel-2MSI, VENμS, and Landsat OLI. An error matrix was derived to determine the level of agreement between the training and testing data. An error matrix is a tally table with columns representing reference data and the rows representing classified data. The major diagonals in the table indicate the agreement between the two datasets. In this regard, overall accuracy (OA) of a particular classification was calculated by dividing the sum of the entries that form the major diagonal (i.e., the sum of correct classifications) by the total number of samples of the entire dataset. The user accuracy (UA) is computed by dividing the correctly classified class-specific samples by the class column's total, and it is expressed as a percentage. Meanwhile, the producer accuracy (PA) is calculated by a specific class's being correctly classified by the row's total, and it is also expressed as a percentage. Story and Congalton [32] detail the entire procedure. Furthermore, Pontius Jr. and Millones's [33] quantity disagreement and allocation disagreement were used in characterizing the performance, as well as the strength of the HyspIRI's spectral settings in relation to that of Sentinel-2MSI, VENμS, and Landsat OLI. In addition, McNemar's test was used to test for significant differences in the performance of different sensors.

3. Results

The ANOVA results showed that there were significant differences ($p = 0.005$) between the healthy, intermediately infected, and severely infected maize crops, based on data resampled to the spectral settings of HyspIRI, Sentinel-2MSI, VENμS, and Landsat OLI. Figure 3 illustrates the differences in the means of healthy, intermediately infected, and severely infected maize crops. Windows of spectral separability between the reflectance of healthy, intermediately infected, and severely infected maize crops were exhibited in the red-edge, as well as in the near-infrared sections of the EMS, based on the spectral settings of all the sensors (Figure 3). There were less windows of spectral separability where healthy maize could be spectrally discriminated from that which was intermediately and highly infected in the visible section of the EMS cover by the four sensors (Figure 3).
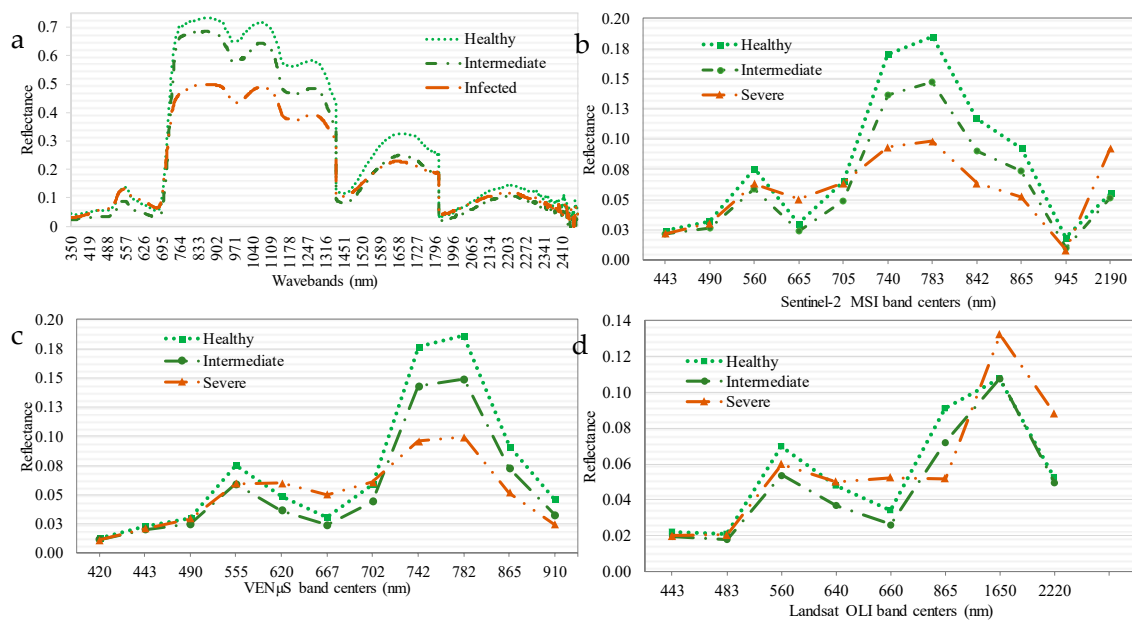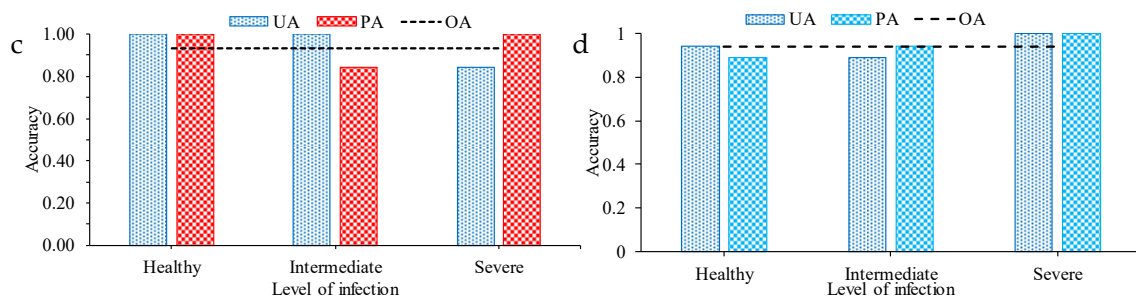
Figure 3. Differences in mean reflectance of healthy, intermediately infected, and severely infected maize crops based on (**a**) HyspIRI, (**b**) Sentinel-2 MSI, (**c**) VENμS, and (**d**) Landsat OLI spectral settings.

In discriminating between the different stages of GSL infection on maize, using PLS–DA, our results indicated that HyspIRI exhibited higher classification accuracies in relation to the other sensors considered in this study (Figure 4). Specifically, HyspIRI exhibited an overall accuracy of 0.99 and a producer and user accuracy of 99% for the healthy and severely infected maize crops. The user accuracy of the intermediately infected crops exhibited a slightly lower user accuracy of 0.94, in relation to the other two infection levels. When using Sentinel-2 MSI spectral settings, accuracies comparable to those of HyspIRI were obtained (overall accuracy 0.95). Only the user accuracies for the intermediately and severely infected were below 0.95 when Sentinel 2 MSI spectral settings were used. A similar trend was observed when using the spectral settings of VENμS sensor. However, the user accuracies for the intermediately and severely infected further decreased to less than 0.9 when VENμS spectral settings were used. The VENμS spectral setting yielded an overall classification accuracy of 0.94. A different trend was observed when using the Landsat 8 OLI spectral settings. High user and producer accuracies of 1.0 were exhibited by the Landsat OLI spectral settings for the severely infected maize crops, whereas those for the healthy and the intermediately infected maize crops were relatively lower than those exhibited by the HyspIRI, Sentinel-2 MSI, and VENμS spectral settings. The overall accuracy exhibited by Landsat 8 OLI was 0.89.
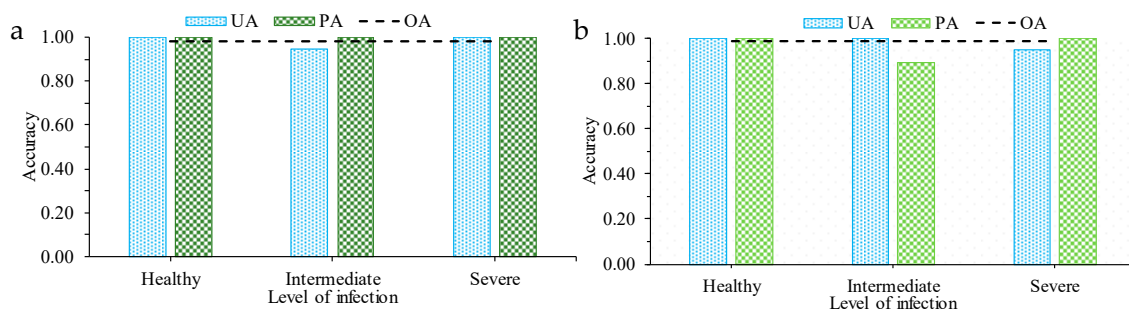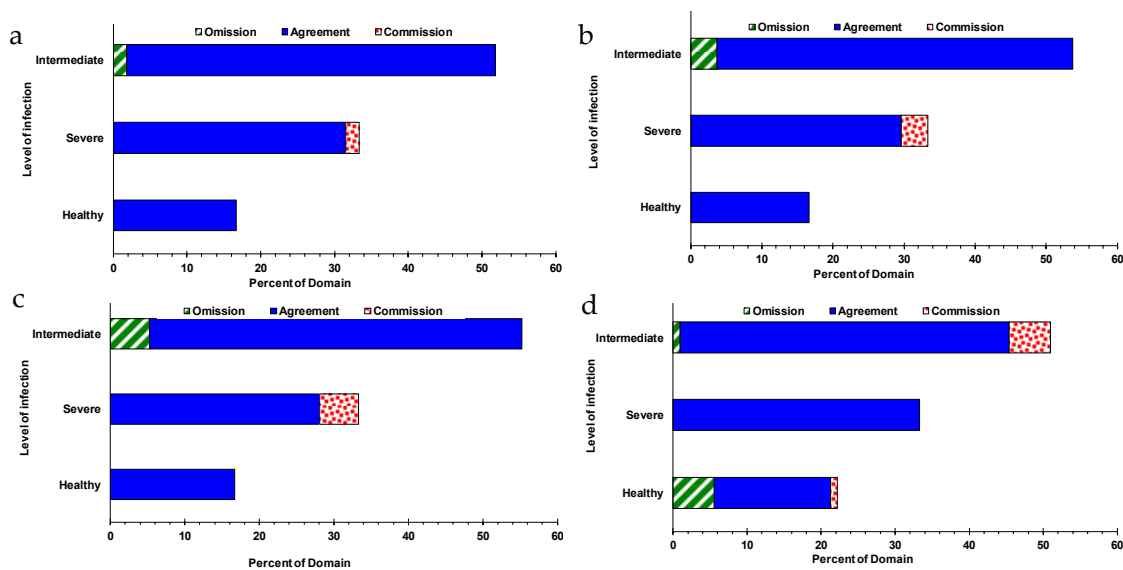

Figure 4. *Cont.*

Figure 4. PLS–DA classification accuracies of healthy, intermediately infected, and severely infected maize crops based on (**a**) HyspIRI, (**b**) Sentinel-2 MSI, (**c**) VENμS, and (**d**) Landsat OLI spectral settings. OA, UA, and PA refer to overall accuracy, user accuracy, and producer accuracies, respectively.

When assessing the accuracy and strength of HyspIRI spectral configurations in relation to those of Sentinel-2MSI, VENμS, and Landsat OLI, based on the allocation of agreement commission and omission, results of this study showed that HyspIRI was stronger and more accurate in discriminating different GLS levels in maize crops (Figure 5). Specifically, HyspIRI exhibited less than 5% allocations of disagreement (commission) for the infected only and optimal allocations of agreement for all the GLS infection levels (Figure 5). Again, a similar trend was of a considerable magnitude of the allocation of disagreement (omission) was observed based on the Sentinel-2 MSI and VENμS sensor settings for the severely 'infected' maize crops. When using Sentinel-2 MSI sensor's settings, the omission increased to above 5% and to about 8%, when using the spectral setup of VENμS sensor. When Landsat OLI's spectral setup was used, the magnitude of omission and commission for the healthy and intermediately infected maize crops increased significant by a magnitude above 10% combined.


Figure 5. Accuracies of healthy, intermediately infected, and severely infected maize crops, based on (**a**) HyspIRI, (**b**) Sentinel-2 MSI, (**c**) VENμS, and (**d**) Landsat OLI spectral settings based on Pontius and Millionres's omission and commission and agreement allocations. See comment on Figure 3 caption.

The most optimal wavebands that were instrumental and influential in making HyspIRI stronger and better in discriminating between different levels of GLS infections in maize were from the red, red-edge, mid, and far infrared spectral regions (Figure 6a). Specifically, the NIR and FIR wavebands between 750 and 800 nm, as well as between 1995 and 2065 nm, followed by the red-edge section, were the highest in terms of variable importance in projection scores when using HyspIRI's spectral settings, as illustrated on Figure 6a. When Sentinel-2 MSI spectral settings were used, the NIR band centered at 945 nm and the red-edge band centered at 740 nm, as well as the NIR bands centered at

783, 842, and 865 nm, were the most influential variables (Figure 6b). Again, VENμS's wavebands from the red-edge and NIR region centered at 945, 740, 842, and 783 nm, in order of importance, were the most influential variables in discriminating between different levels of GLS infections on maize crops (Figure 6c). Meanwhile, Landsat OLI's bands 7, 4, 5, and 6 were the most influential variables, as illustrated in Figure 6d.
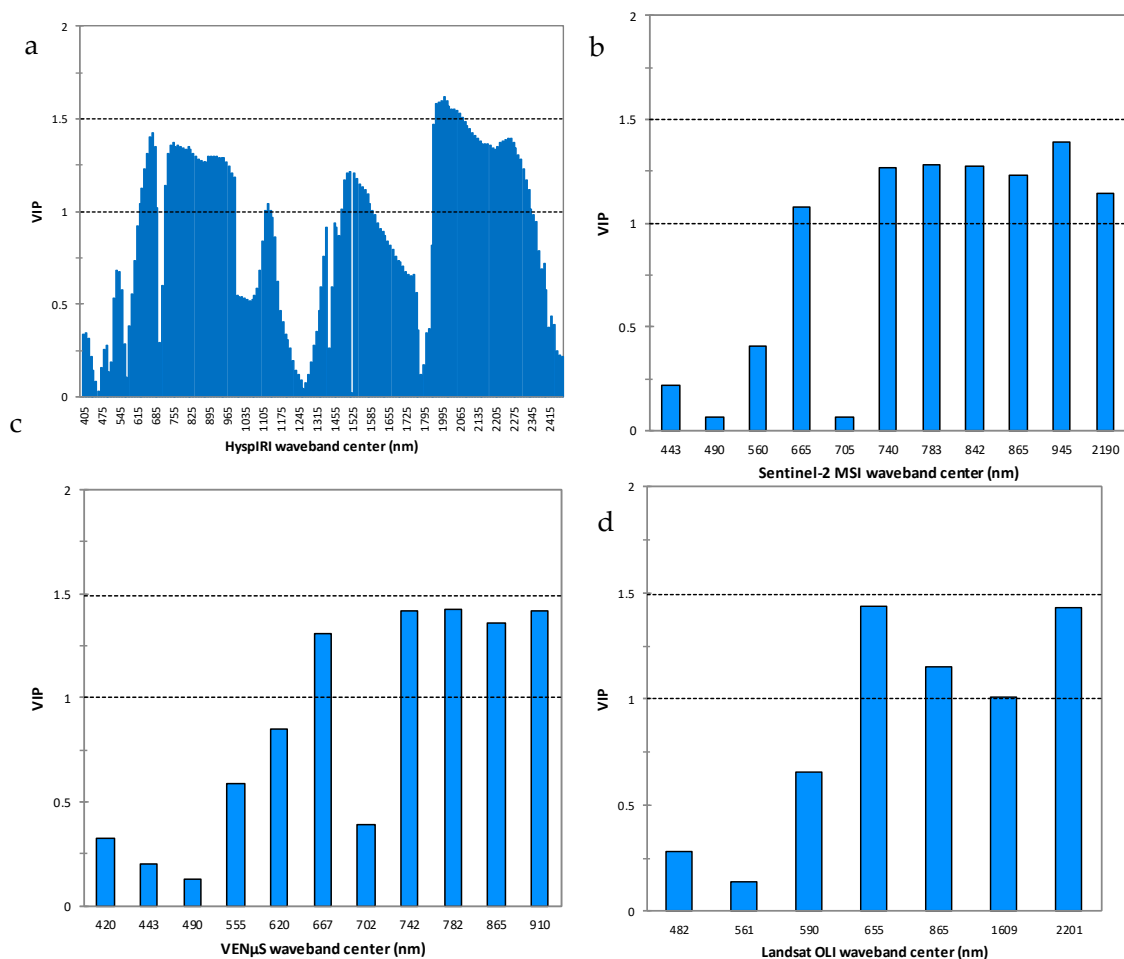
Figure 6. Variable importance in projection scores for (**a**) HyspIRI, (**b**) Sentinel-2 MSI, (**c**) VENμS, and (**d**) Landsat OLI spectral bands. The black lines represent the optimal level of the variable importance projection score determined, based on the literature [34].

4. Discussion

The spectral setup of HyspIRI was more robust and accurate in classifying healthy maize crops from those that were intermediately, as well as severely, infected by GLS, in relation to the spectral settings of Sentinel-2MSI, VENμS, and Landsat OLI. The literature underscores the narrow widths of hyperspectral wavebands in vegetation discrimination as the reason for their optimal performance when compared with broad wavebands, which tend to mask critical fine-grained information that is instrumental in discriminating between infected crops and healthy ones [18,19,35]. This explains the optimal performance of HyspIRI in relation to the other three sensors.

Specifically, Sentinel-2MSI, VENμS, and Landsat OLI have broader wavebands characterized by widths which range from 15 to 115 nm. These wavebands tend to be insensitive to the optical traits that are altered by diseases such as the GLS, resulting in their being insensitive to the infected crop's optical canopy traits. This explains the less accuracies exhibited by sensors such as Landsat OLI in this study. In a similar study, Dhau, et al. [5] illustrated the utility of hyperspectral data in discriminating

maize crops that were under different levels of maize-streak virus infections. Specifically, they attained an overall accuracy of 95.83%, which is similar to that demonstrated by HyspIRI in this study.

Results in this study showed that the performance of resampled Sentinel-2 MSI was comparable to that of HyspIRI, but was not significantly different from that of VENµS. However, Sentinel-2 MSI performed better than Landsat OLI, which exhibited the least classification accuracies. Although Sentinel-2 MSI does not have spectral channels that are as narrow as those of HyspIRI, it covers the red-edge section, which are not covered by Landsat OLI sensor. This could explain the optimal performance of Sentinel-2 when compared to Landsat OLI sensor's spectral setup. When comparing the spectral setup of Sentinel-2 MSI, there were slightly less variations in terms of the EMS regions covered by both these sensors, hence their almost-similar performance in discriminating between different levels of GSL disease in this study. Above all, the band widths of Landsat OLI, when compared to those of Sentinel-2 MSI, are slightly broad, masking even more information that is critical in discriminating maize crops at various GLS-infection levels. Results of this study validate the theoretical discourse put forth by Marshall and Thenkabail [19] which emphasizes the importance of high spectral resolution as opposed to high spatial resolution, particularly on sensors that cover the red-edge section of the EMS when HypIRI outperformed Sentinel-2MSI, VENµS, and Landsat OLI.

Resampled HyspIRI's NIR and red-edge bands were more influential variables in discriminating between maize crops under different levels of GLS infections. The optimal performance of HyspIRI's spectral settings could be explained by its contiguous 10 nm narrow wavebands, which are sensitive in detecting the subtle changes in the biochemical and physiological changes induced by the GLS on maize crops. The GSL disease manifests as black spots, which attack the stomatal activity and then later on develop into long rectangular-shaped grey-to-tan-colored lesions. These changes alter the optical foliar traits, particularly the pigment concentrations and chlorophyll content, into rectangular-shaped grey-to-tan lesions. When chlorophyll and pigment concentrations are reduced, infected maize crops become very discriminable from those that are healthy, as well as those under the initial and intermediate infection stages, particularly in the NIR and the red-edge regions [11,12]. Healthy plants with high chlorophyll concentrations tend to reflect highly on the NIR, whereas the chlorophyll concentrations shift the red-edge position toward the longer wavebands, facilitating an optimal discrimination based on the narrow spectra channels. Meanwhile, the GLS lesions in infected maize crop leaves reduce chlorophyll concentration, which then shifts the red-edge position toward the short wavebands, facilitating optimal discriminations based on the red-edge section of the EMS, especially when using narrower spectral channels in relation to broad wavebands. In a similar study, Dhau et al. [5] showed that the highly influential wavebands in discriminating maize crops under various stages of maize-streak virus infections were from the NIR (881 and 2338 nm) and visible (552 and 603 nm) spectral sections of the EMS, using proximal sensed data. Al-Ahmadi, et al. [36], in a related study, demonstrated that the narrow spectral channels of hyperspectral data, particularly the NIR 1940 band, optimally detected *Macrophomina phaseolina* toxin effects in soybeans, as was the case in this study. Results of these studies illustrate and concur with those of the present study, which noted that the visible (red-edge) and the NIR sections of the EMS are critical for characterizing different levels of crop infections by diseases such as GLS.

In assessing the spectral separability of the three different levels of GLS infections based on the resampled HyspIRI, Sentinel-2MSI, VENµS, and Landsat OLI data, results showed that there were less windows for spectrally discriminating between healthy maize and intermediately and highly infected maze in the visible section of the EMS by the four sensors. This could be attributed to the fact that the visible section of the EMS is highly susceptible to atmospheric influences. Atmospheric influences result in the attenuation and dilution of the signal, making the spectral discrimination of different levels of GLS-infected maize futile, based on the bands from the visible section of the EMS covered by resampled HyspIRI, Sentinel-2MSI, VENµS, and Landsat OLI data in this study.

Implications of Utilizing Simulated HyspIRI Spectral Settings

Despite the optimal performance and success exhibited by HyspIRI in discriminating maize crops grown under different levels of GLS infection in relation to Sentinel-2MSI, VENµS, and Landsat OLI based on simulated data, there is still a need to assess this sensor's satellite-borne measured data. Considering the fact that this study intended to only assess the spectral configuration of these sensors, there is a need to assess the effect of their radiometric and spatial resolutions in a similar application setup. Largely, the satellite-borne reflectance remotely sensed data tend to be affected by numerous factors associated with the sensor's platform (i.e., the zenith angle of the sensor and speed of the platform) and atmospheric-related influences (i.e., presence of atmospheric impurities, haze, and sun irradiance). Spectrometric-proximally sensed data tends to be less affected by atmospheric related influences and has a different sun angle (i.e., a beam divergence is of ±60°); hence, it offers a robust dataset that is suitable for testing the usability and strength of forthcoming sensor missions, such as HyspIRI's spectral band settings. Meanwhile, HyspIRI will have a lower signal-to-noise ratio of 700:1 at 600 nm and 500:1 at 2200 nm when compared to ASD FieldSpec, which ranges between 700:1 and 2100:1 for 350–2500 nm [23]. Although the ground sampling distance of 30 m could be regarded as moderate, the literature illustrates that it is optimal for characterizing crop physiology [37–39]. For example, Mfuka et al. [37] were able to characterize white mold pathogen on soybeans to optimal overall accuracies of 95%–99%, based on the ground sampling distance of 30 m characteristic of Landsat OLI data. In this regard, the 30 m ground sampling distance is deemed effective for agronomical management of the diseases such as GLS. However, the performance of these sensors', namely, HyspIRI, Sentinel-2MSI, VENµS, and Landsat OLI spatial and spectral settings derived using satellite platforms, still needs to be evaluated in a similar environment.

5. Conclusions

We tested the strength and practicality of HyspIRI's spectral configuration in detecting and discriminating between maize crops at various stages of GLS-disease infection in relation to that of Sentinel-2MSI, VENµS, and Landsat OLI. Grounded on the findings of this study, we conclude that.

HyspIRI's spectral setup is more robust and effective in characterizing maize crops growing under different levels of GLS-disease infection when compared to Sentinel-2MSI, VENµS, and Landsat OLI-2.

Sentinel-2 MSI could be a better alternative to HyspIRI, considering the fact that its spectral setup performed comparable to that of HyspIRI in discriminating maize crops with different levels of GLS infections.

This study illustrates that HyspIRI hyperspectral remotely sensed data could be a panacea to the lack of spatially explicit spectral resolution data as a better alternative for accurate and effective monitoring and forecasting of agricultural-crop diseases similar to the GSL, which are severe yield-reduction agents. Furthermore, results of this work are a significant step toward achieving urgently required techniques for comprehensively assessing, monitoring, and forecasting food-crop disease epidemics at relatively larger scales. These techniques effectively build on initiatives for improving food-crop production, while addressing the global village's mandate of achieving food security, especially for developing nations, which are more susceptible to frequent droughts, limited resources, and poverty. Notwithstanding the soundness of this study's findings, there is still need to assess the spectral settings of these sensors on different crops and physical settings. Above all, there is still a need to test the actual remotely sensed products of these sensors in effectively monitoring and forecasting agricultural-crop diseases. There is also need to assess the performance of vegetation indices of these sensors in discriminating maize crops at various stages of GLS diseases infection.

References

1.　Mahuku, G.; Lockhart, B.E.; Wanjala, B.; Jones, M.W.; Kimunye, J.N.; Stewart, L.R.; Cassone, B.J.; Sevgan, S.; Nyasani, J.O.; Kusia, E. Maize Lethal Necrosis (Mln), an Emerging Threat to Maize-Based Food Security in Sub-Saharan Africa. *Phytopathology* **2015**, *105*, 956–965. [CrossRef] [PubMed]

2.　Dhami, N.B.; Kim, S.K.; Paudel, A.; Shrestha, J.; Rijal, T.R. A Review on Threat of Gray Leaf Spot Disease of Maize in Asia. *J. Maize Res. Dev.* **2015**, *1*, 71–85. [CrossRef]

3.　Ward, J.M.J.; Birch, E.B.; Nowel, D.C. *Grey Leaf Spot on Maize*; Cedara Agricultural Develop Institute: Pietermaritzburg, South Africa, 1994.

4.　Geis, J.P. Application and Timing Effects of Qoi and Dmi Fungicides and a Foliar Fertilizer on Overall Plant Health and Grain Yield in Corn. Master's Thesis, Purdue University, West Lafayette, IN, USA, 2014.

5.　Dhau, I.; Adam, E.; Mutanga, O.; Ayisi, K.K. Detecting the Severity of Maize Streak Virus Infestations in Maize Crop Using in Situ Hyperspectral Data. *Trans. R. Soc. S. Afr.* **2018**, *73*, 8–15. [CrossRef]

6.　Gao, F.; Anderson, M.C.; Zhang, X.; Yang, Z.; Alfieri, J.G.; Kustas, W.P.; Mueller, R.; Johnson, D.M.; Prueger, J.H. Toward Mapping Crop Progress at Field Scales through Fusion of Landsat and Modis Imagery. *Remote Sens. Environ.* **2017**, *188*, 9–25. [CrossRef]

7.　Lowe, A.; Harrison, N.; French, A.P. Hyperspectral Image Analysis Techniques for the Detection and Classification of the Early Onset of Plant Disease and Stress. *Plant Methods* **2017**, *13*, 80. [CrossRef]

8.　Bégué, A.; Arvor, D.; Bellon, B.; Betbeder, J.; Abelleyra, D.D.; Ferraz, R.P.D.; Lebourgeois, V.; Lelong, C.; Simões, M.; Verón, S.R. Remote Sensing and Cropping Practices: A Review. *Remote Sens.* **2018**, *10*, 99. [CrossRef]

9.　Thenkabail, P.S.; Smith, R.B.; Pauw, E.D. Evaluation of Narrowband and Broadband Vegetation Indices for Determining Optimal Hyperspectral Wavebands for Agricultural Crop Characterization. *Photogram. Eng. Remote Sens.* **2002**, *68*, 607–622.

10.　Mulla, D.J. Twenty Five Years of Remote Sensing in Precision Agriculture: Key Advances and Remaining Knowledge Gaps. *Biosyst. Eng.* **2013**, *114*, 358–371. [CrossRef]

11.　Mee, C.Y.; Balasundram, S.K.; Hanif, A.H.M. Detecting and Monitoring Plant Nutrient Stress Using Remote Sensing Approaches: A Review. *Asian J. Plant Sci.* **2017**, *16*, 1–8.

12.　Chaerle, L.; Straeten, D.V.D. Imaging Techniques and the Early Detection of Plant Stress. *Trends Plant Sci.* **2000**, *5*, 495–501. [CrossRef]

13.　Herrmann, I.; Bdolach, E.; Montekyo, Y.; Rachmilevitch, S.; Townsend, P.A.; Karnieli, A. Assessment of Maize Yield and Phenology by Drone-Mounted Superspectral Camera. *Precis. Agric.* **2019**, 1–26. [CrossRef]

14.　Herrmann, I.; Vosberg, S.; Ravindran, P.; Singh, A.; Chang, H.X.; Chilvers, M.; Conley, S.; Townsend, P. Leaf and Canopy Level Detection of Fusarium Virguliforme (Sudden Death Syndrome) in Soybean. *Remote Sens.* **2018**, *10*, 426. [CrossRef]

15.　Mahlein, A.K. Plant Disease Detection by Imaging Sensors–Parallels and Specific Demands for Precision Agriculture and Plant Phenotyping. *Plant Dis.* **2016**, *100*, 241–251. [CrossRef] [PubMed]

16.　Mahlein, A.K.; Kuska, M.T.; Behmann, J.; Polder, G.; Walter, A. Hyperspectral Sensors and Imaging Technologies in Phytopathology: State of the Art. *Ann. Rev. Phytopathol.* **2018**, *56*, 535–558. [CrossRef]

17.　Zhang, M.; Qin, Z.; Liu, X.; Ustin, S.L. Detection of Stress in Tomatoes Induced by Late Blight Disease in California, USA, Using Hyperspectral Remote Sensing. *Int. J. Appl. Earth Obs. Geoinf.* **2003**, *4*, 295–310. [CrossRef]

18. Thenkabail, P.S.; Mariotto, I.; Gumma, M.K.; Middleton, E.M.; Landis, D.R.; Huemmrich, K.F. Selection of Hyperspectral Narrowbands (Hnbs) and Composition of Hyperspectral Twoband Vegetation Indices (Hvis) for Biophysical Characterization and Discrimination of Crop Types Using Field Reflectance and Hyperion/Eo-1 Data. *IEEE J. Sel. Top. Appl. Earth Obs. Remote Sens.* **2013**, *6*, 427–439.

19. Marshall, M.; Thenkabail, P. Advantage of Hyperspectral Eo-1 Hyperion over Multispectral Ikonos, Geoeye-1, Worldview-2, Landsat Etm+, and Modis Vegetation Indices in Crop Biomass Estimation. *ISPRS J. Photogram. Remote Sens.* **2015**, *108*, 205–218. [CrossRef]

20. Maimaitiyiming, M.; Ghulam, A.; Bozzolo, A.; Wilkins, J.L.; Kwasniewski, M.T. Early Detection of Plant Physiological Responses to Different Levels of Water Stress Using Reflectance Spectroscopy. *Remote Sens.* **2017**, *9*, 745. [CrossRef]

21. Mariotto, I.; Thenkabail, P.S.; Huete, A.; Slonecker, E.T.; Platonov, A. Hyperspectral Versus Multispectral Crop-Productivity Modeling and Type Discrimination for the Hyspiri Mission. *Remote Sens. Environ.* **2013**, *139*, 291–305. [CrossRef]

22. Calderón, R.; Navas-Cortés, J.A.; Zarco-Tejada, P.J. Early Detection and Quantification of Verticillium Wilt in Olive Using Hyperspectral and Thermal Imagery over Large Areas. *Remote Sens.* **2015**, *7*, 5584–5610. [CrossRef]

23. Lee, C.M.; Cable, M.L.; Hook, S.J.; Green, R.O.; Ustin, S.L.; Mandl, D.J.; Middleton, E.M. An Introduction to the Nasa Hyperspectral Infrared Imager (Hyspiri) Mission and Preparatory Activities. *Remote Sens. Environ.* **2015**, *167*, 6–19. [CrossRef]

24. Green, R.O. Global Vswir Imaging Spectroscopy and the 2017 Decadal Survey. In Proceedings of the IGARSS 2018-2018 IEEE International Geoscience and Remote Sensing Symposium Valencia, Valencia, Spain, 22–27 July 2018.

25. EnMAP_Ground_Segment_Team. Spaceborne Imaging Spectroscopy Mission Compilation. In *Spaceborne Imaging Spectroscopy EO Missions*; Pinnel, N., Ed.; German Aerospace Center (DLR): Potsdam, German, 2009; pp. 1–25. Available online: http://www.enmap.org/sites/default/files/pdf/Hyperspectral_EO_Missions_2019_06_03.pdf (accessed on 30 October 2019).

26. Jo, Y.H.; Kim, H.C.; Hu, C.; Klemas, V.V.; Turpie, K.R. Potential Applications of Hyspiri for the Observation of Sea-Margin Processes. *J. Coastal Res.* **2019**, *35*, 227–239.

27. Korsman, J.; Meisel, B.; Kloppers, F.J.; Crampton, B.G.; Berger, D.K. Quantitative Phenotyping of Grey Leaf Spot Disease in Maize Using Real-Time Pcr. *Eur. J. Plant Pathol.* **2012**, *133*, 461–471. [CrossRef]

28. Ward, J.M.; Stromberg, E.L.; Nowell, D.C.; Nutter, F.W., Jr. Gray Leaf Spot: A Disease of Global Importance in Maize Production. *Plant Dis.* **1999**, *83*, 884–895. [CrossRef]

29. Hestir, E.L.; Brando, V.E.; Bresciani, M.; Giardino, C.; Matta, E.; Villa, P.; Dekker, A.G. Measuring Freshwater Aquatic Ecosystems: The Need for a Hyperspectral Global Mapping Satellite Mission. *Remote Sens. Environ.* **2015**, *167*, 181–195. [CrossRef]

30. Prasad, S.; Bruce, L.M.; Kalluri, H. Data Exploitation of Hyspiri Observations for Precision Vegetation Mapping. In Proceedings of the 2009 IEEE International (IGARSS), Cape Town, South Africa, 12–17 July 2009.

31. Samiappan, S.; Prasad, S.; Bruce, L.M.; Robles, W. Nasa's Upcoming Hyspiri Mission—Precision Vegetation Mapping with Limited Ground Truth. In Proceedings of the 2010 IEEE International Geoscience and Remote Sensing Symposium, Honolulu, HI, USA, 25–30 July 2010.

32. Story, M.; Congalton, R.G. Accuracy Assessment: A User's Perspective. *Photogram. Eng. Remote Sens.* **1986**, *52*, 397–399.

33. Pontius, J.; Gilmore, R.; Millones, M. Death to Kappa: Birth of Quantity Disagreement and Allocation Disagreement for Accuracy Assessment. *Int. J. Remote Sens.* **2011**, *32*, 4407–4429. [CrossRef]

34. Olden, J.D.; Joy, M.K.; Death, R.G. An Accurate Comparison of Methods for Quantifying Variable Importance in Artificial Neural Networks Using Simulated Data. *Ecol. Model.* **2004**, *178*, 389–397. [CrossRef]

35. Mutanga, O.; Aardt, J.V.; Kumar, L. Imaging Spectroscopy (Hyperspectral Remote Sensing) in Southern Africa: An Overview. *S. Afr. J. Sci.* **2009**, *105*, 193–198. [CrossRef]

36. Al-Ahmadi, A.H.; Subedi, A.; Wang, G.; Choudhary, A.; Watson, D.G. Detection of Charcoal Rot (Macrophomina Phaseolina) Toxin Effects in Soybean (Glycine Max) Seedlings Using Hyperspectral Spectroscopy. *Comput. Electron. Agric.* **2018**, *150*, 188–195. [CrossRef]

37. Mfuka, C.; Zhang, X.; Byamukama, E. Mapping and Quantifying White Mold in Soybean across South Dakota Using Landsat Images. *J. Geogr. Inf. Syst.* **2019**, *11*, 331–346. [CrossRef]

38. Chen, X.; Ma, J.; Qiao, H.; Cheng, D.; Xu, Y.; Zhao, Y. Detecting Infestation of Take-All Disease in Wheat Using Landsat Thematic Mapper Imagery. *Int. J. Remote Sens.* **2007**, *28*, 5183–5189. [CrossRef]
39. Jin, X.; Ma, J.; Wen, Z.; Song, K. Estimation of Maize Residue Cover Using Landsat-8 Oli Image Spectral Information and Textural Features. *Remote Sens.* **2015**, *7*, 14559–14575. [CrossRef]